

Article

# Performance Analysis and Structure Optimization of a Nautilus Isometric Spiral Wind Turbine

Zheng Li <sup>1,\*</sup> , Wenda Zhang <sup>1</sup>, Hao Dong <sup>1</sup> and Yongsheng Tian <sup>2</sup>

<sup>1</sup> School of Electrical Engineering, Hebei University of Science and Technology, Shijiazhuang 050018, China; zhangwenda@stu.hebust.edu.cn (W.Z.); donghao@stu.hebust.edu.cn (H.D.)

<sup>2</sup> Jilantai Town Precision Salt Branch Factory, Azuo Banner 750333, China; yongshengt@126.com

\* Correspondence: lizheng@hebust.edu.cn

Received: 22 November 2019; Accepted: 23 December 2019; Published: 25 December 2019



**Abstract:** Background: This paper proposes a Nautilus isometric spiral vertical axis wind turbine, which is a new structure, and its aerodynamic performance and power generation performance need to be analyzed. Methods: A 3D model of the wind turbine was built and its aerodynamic performance was analyzed. Then the wind turbine power generation and grid-connected simulation platform was built by MATLAB/SIMULINK, and its power generation performance and subsequent grid connection were studied. Results: The basic parameters of the wind turbine were obtained. In order to improve efficiency, parameters such as pressure, torque, wind energy utilization rate and relative velocity of wind turbines with different blade numbers and different sizes were compared. In addition, by building a simulation platform for the power generation control system, the power generation characteristics and grid connection characteristic curves of the generator were obtained. Conclusions: When the number of blades is three and the ratio between the ellipse major axis and minor axis of the blade inlet is 0.76, the best efficiency of the wind turbine can be obtained. Application of the power generation control system used in this paper can achieve grid-connected operation of this wind turbine. It also confirmed that the Nautilus isometric spiral wind turbine has good performance and is worthy of in-depth research.

**Keywords:** vertical axis wind turbine; aerodynamic performance; power generation characteristics

## 1. Introduction

Wind energy has become the focus of renewable energy research worldwide, and many countries use wind power as the basis for their long-term plans related to the environment [1,2]. The use of wind energy mainly depends on wind turbines. There are two types of wind turbines: horizontal axis wind turbines (HAWT) and vertical axis wind turbines (VAWT). After several decades of research on HAWTs, power generation technology is considered mature and has been widely used in large power plants. In recent years, VWATs have become the focus of research scholars. VWATs play an important role in supplementing energy, structural adjustments in the energy industry, and capturing wind energy in low wind speed areas due to their own advantages [3].

At present, most researchers use numerical simulation methods to analyze the aerodynamic performance of vertical axis wind turbines. The characteristics of the VWAT were demonstrated and compared with the HAWT, and the advantages and disadvantages of the two types of wind turbines were emphasized [4]. In [5], a new dual-rotor wind turbine was proposed, and the effect of the air boundary layer on the aerodynamic performance of the wind turbine was analyzed by numerical simulation. Based on the lift line simulation method, the design of the megawatt wind turbine was completed, and aerodynamic factors were considered in the design process. The effects of different vertical axis wind turbines on aerodynamic performance during the design process were

studied [6]. References [4–6] carried out an in-depth analysis of the aerodynamic performance of wind turbines by numerical simulation methods, but these analyses can only provide a general understanding of the performance parameters of wind turbines, and cannot greatly improve the performance. In order to improve the wind energy conversion efficiency of vertical axis wind turbines, some researchers have designed new wind turbines with better performance. In the design process of wind turbines, the most commonly used design method is numerical simulation, which is the main application method of this article. In [7], a fish-shaped airfoil vertical axis wind turbine was proposed, and it was proved by 3D numerical simulation that it has a good aerodynamic performance curve. The numerical simulation method can be used to explore the influence of a baffled wind wheel structure on aerodynamic performance, and analyze parameters such as overlap ratio, blade curvature, baffle length and installation angle. It was confirmed that this structure can indeed improve the wind energy utilization rate of wind turbines [8]. In [9], an S-type and H-type combined vertical axis wind turbine was proposed, and the start-up and aerodynamic performance of the combined wind turbine was analyzed by the CFD method. This combined wind turbine has superior performance than a single H-type wind turbine, with a maximum wind energy utilization rate of 0.298 [9]. Although the literature [7–9] proposed a relatively new type of vertical axis wind turbine structure, the structural parameters of the new wind turbine have not been optimized. The tangential forces generated by the NACA0012, NACA0015, NACA0018 and NACA0021 airfoil types under different lift-resistance coefficients were analyzed, which can be used to study the torque performance of the 4-blade Darrieus rotor type VAWT [10]. The numerical methods were used to study the four trailing edge profiles of the two-dimensional model, namely acute angles, rounded corners, S-blunt and R-blunt, to verify whether the performance of the straight blade vertical axis wind turbine was affected when the trailing edge profiles were different [11]. The literature [10,11] has carried out an in-depth analysis of the airfoil of wind turbine blades. At present, the research on the airfoil of vertical axis wind turbines is mainly focused on the research of lift wind turbines, and the research on resistance wind turbines is rare. Aiming at the problem that the conversion efficiency of the Savonius-type vertical axis wind turbine is not high, a Savonius wind turbine with elliptical blades was proposed, and analyzed the blade flatness of Impact of wind turbine wind energy conversion efficiency. The results show that such blades can greatly improve wind turbine performance [12]. This effect on blade ellipse flatness is one of the factors affecting the performance of resistance wind turbines, and it is also one of the research focuses in this paper. In order to understand the effect of pitch angle  $\beta$  on the performance of vertical-axis wind turbines with straight blades, a two-dimensional numerical analysis of the unsteady  $k-\omega$  turbulence model using sliding grid technology was carried out. It is found that the negative angle installation method can improve the running performance of the wind wheel and increase the power coefficient of the wind rotor, and the experiment verified the correctness of the results [13]. The effect of the number of blades on the aerodynamic performance of a wind turbine can be analyzed by the CFD method. The results show that the change in the number of blades has a great impact on power. When the number of blades is five, the best wind energy conversion efficiency can be obtained. Reference [13] optimized the structural parameters of wind turbines, and [14] compared wind turbines with different blade numbers, but did not comprehensively analyze the optimization analysis of blade numbers and structural parameters. In [15], a towed vertical axis wind turbine was proposed. The aerodynamic model was used to analyze the pressure distribution of the blade through three-dimensional numerical simulation. The optimal vertical axis wind turbine configuration is obtained by comparing the torque factor and power factor of the blade configuration with differences. At the same time, the performance of different blade numbers was also analyzed. At the same time, the performance of different numbers of blades was compared and analyzed, but this article is mainly aimed at Senegalese lift wind turbines. In [16,17], the in-depth research on wind turbine power generation and grid-connected control systems was conducted. These studies are also very valuable, but their disadvantage is that they do not target specific wind turbines.

This paper introduces a Nautilus isometric spiral vertical axis wind turbine. As a new type of resistance-type vertical axis wind turbine, there has been little research on this wind turbine. Combined with the understanding and analysis of the above literatures, the research content of this article is very extensive, and the specific analysis content is as follows:

First, a 3D wind turbine model is constructed by finite element simulation software. Basic parameters such as wind energy utilization and torque are analyzed. In order to obtain higher efficiency, the pressure contour, torque, wind energy utilization rate, relative velocity of the wind wheel with 2, 3, 4 and 5 blades were studied. After the optimal number of blades was determined, the structural parameters were further optimized by changing the ratio of the major axis to the minor axis of the ellipse of the impeller inlet, and comparing the torque, wind energy utilization rate and relative velocity. Then use MATLAB/SIMULINK to build a mathematical model of the generator and analyze its power generation characteristics. Finally, the actual power of the wind turbine was measured by an established wind turbine prototype. By comparing actual data with simulation data, the effectiveness and feasibility of the Nautilus isometric spiral wind turbine is verified.

## 2. Wind Turbine Model

### 2.1. Basic Parameters

According to Newton's second law [15,18]:

$$F = ma, \quad (1)$$

$$E = \frac{1}{2}mv^2, \quad (2)$$

The above equations are all effective when the mass is constant, but the mass of the wind is an ever-changing amount with different velocities at different times. Therefore, the dynamic equation of the wind is:

$$P = \frac{dE}{dt} = \frac{1}{2} \frac{dm}{dt} v_w^2, \quad (3)$$

Replacing  $\frac{dm}{dt}$  in Equation (3) with Equation (4):

$$\frac{dm}{dt} = \rho A v_w, \quad (4)$$

where  $\rho$  is the air density;  $A$  is the sweeping area.

The resulting kinetic energy equation is:

$$P = \frac{dE}{dt} = \frac{1}{2} \rho A v_w^3, \quad (5)$$

The average wind speed  $v_w$  is substituted for  $v$  in Equation (2), and the mechanical power extracted by the wheel of the wind turbine is:

$$P_w = \frac{1}{2} \rho A v_w (v_u^2 - v_d^2), \quad (6)$$

where  $v_u$  is the upstream wind speed of the wind turbine,  $v_d$  is the downstream wind speed of the wind turbine.

The formula for mass conversion is:

$$\rho A v_w = \frac{\rho A (v_u + v_d)}{2}, \quad (7)$$

So Equation (7) can be expressed as:

$$P_w = \frac{1}{2}[\rho A\{\frac{v_u}{2}(v_u^2 - v_d^2) + \frac{v_d}{2}(v_u^2 - v_d^2)\}], \quad (8)$$

$$P_w = \frac{1}{2}\rho A v_u^3 C_p, \quad (9)$$

The formula for calculating wind energy utilization  $C_p$  is:

$$C_p = \frac{P_w}{(1/2)\rho A v_u^3} = \frac{T\omega}{(1/2)\rho A v_u^3}, \quad (10)$$

where  $P_w$  is the shaft power of wind turbine, It can be expressed as:

$$P_w = T\omega, \quad (11)$$

where  $T$  is rotor torque,  $\omega$  is rotor rotational angular velocity.

Torque coefficient  $C_t$  and wind energy utilization  $C_p$  are important parameters for evaluating wind turbine performance. The relationship between the two is:

$$C_t = \frac{C_p}{\lambda} = \frac{T}{(1/2)\rho A R v_u^2}, \quad (12)$$

where  $\lambda$  is the tip speed ratio, It can be expressed as:

$$\lambda = \frac{\omega R}{v_u}, \quad (13)$$

where  $R$  is the radius of the wind wheel.

## 2.2. Modeling, Meshing and Solving

The Nautilus isometric spiral wind turbine is composed of wind wheel, vertical shaft, bearing, bearing seat, coupling, speed increasing box, generator, controller, battery, inverter, etc. Figure 1a shows the overall three-dimensional model of the wind turbine, Figure 1b is the three-dimensional model of the blade, the radial section of the blade is elliptical or symmetrical airfoil or symmetrical isometric spiral type. When a blade is facing away from the wind, there is exactly one side of the blade just facing the wind. At this time, the drag coefficient of the windward blade is large, the drag coefficient of the leeward blade is small, so the thrust generated is large. In addition, the leeward blades extend to the interior of the windward blades for acceleration and guidance. When the wind is drawn to the outside of the windward blade, the wind wheel will be rotated with less force [19]. The specific parameters of the wind turbine are listed in Table 1.

**Table 1.** The specific parameter of the wind turbine.

Parameter	Value	Parameter	Value
Height of the blade	0.3 m	Height of shaft	5 m
Radius of the blade	0.65 m	Radius of shaft	0.2 m
Rated power	300 W	Starting wind speed	1.5–2 m/s

The flow field analysis was performed using the Fluent (CFX) module in the ANSYS Workbench by simulating the operation of the wind turbine in actual operation. This paper focuses on the fluid-solid coupling and aerodynamics of wind turbine 3D models. Figure 2 is a simulation of the static domain and rotational domains of the wind turbine flow field, and Figure 3 is the wind turbine fluid domain boundary setting. The flow field consists of two parts: the static domain and the rotating domain.

The static domain is the external environment in which the wind turbine is located, and the rotating domain is the working environment in which the wind turbine blades operate. In order to simulate the environment in which the wind turbine is located as realistically as possible, the range of the static domain should be much larger than the size of the wind turbine, and the range of the rotating domain is slightly larger than the rotating area of the wind blade. The length of the static region in the X-axis direction is 8.65 m, the length in the Y-axis direction is 3.65 m, the length in the Z-axis direction is 5.5 m, and the three axes of the rotation domain are both 0.2 m larger than the rotation range.

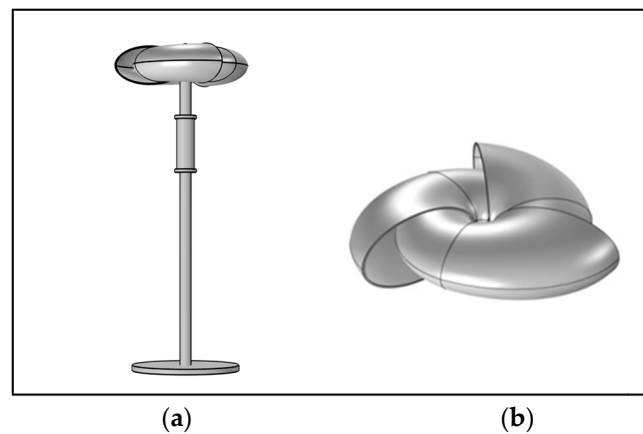


**Figure 1.** (a) The Nautilus isometric spiral wind turbine model; (b) The wind blade model.

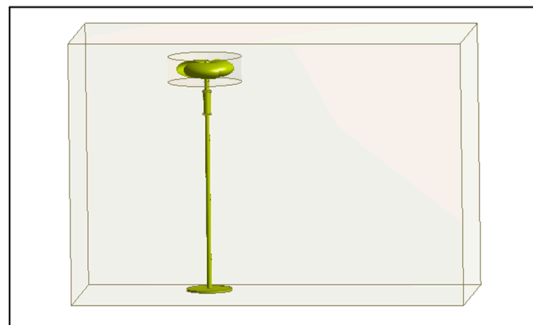


**Figure 2.** The static domain and rotating domain of the wind turbines.

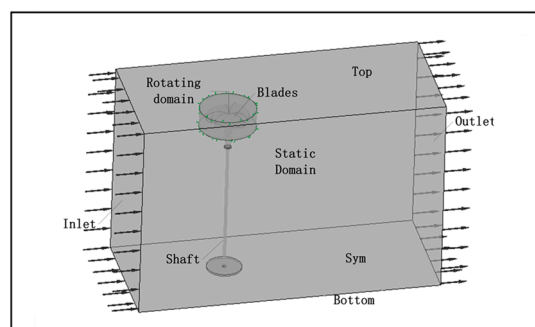


**Figure 3.** Fluid domain boundary setting.

After the model and the flow field are established, the meshing needs to be performed. During the division process, the selected mesh type, grid layout and algorithm will directly affect the accuracy of the numerical simulation results [20]. This paper adopts the automatic mesh generation method, which is a relatively classic mesh division method in software. For some irregular models, this method usually meets the calculation requirements. The whole is a tetrahedral mesh, which has good adaptability to complex geometries. At the irregularities of the model, the grid is relatively dense,

which improves the calculation accuracy. Figure 4 is a schematic diagram of meshing of static domains, rotation domains, and blades. The grid-independent verification is done to make the final result as accurate as possible. The wind speed is set to 5 m/s, the outlet static pressure is 0 Pa, and only the number of meshes is changed to obtain the grid-independent curve. As shown in Figure 5, it can be seen that after the number of meshes reaches 800,000, the torque value tends to be stable, and the results show that when the number of meshes exceeds 800,000, the calculation result is accurate.

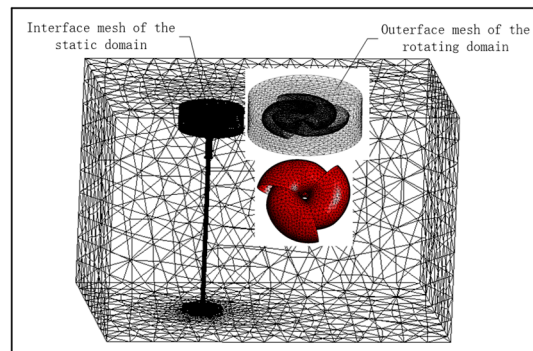


Figure 4. Schematic diagram of meshing.

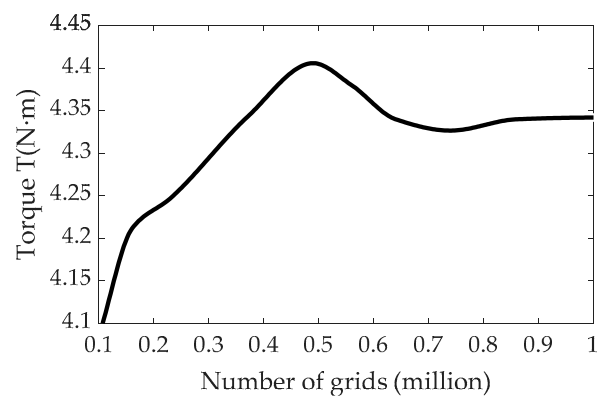


Figure 5. Network independence verification curve.

Figure 6 shows a simplified schematic diagram of wind turbine rotation as a result of wind turbines being affected by wind speed. The wind direction is as shown in Figure 6. From the top view, the rotation direction of the blade is clockwise.

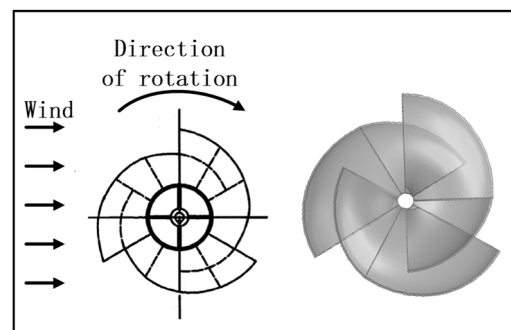


Figure 6. Rotating schematic.

On the basis of the completion of the meshing, the setting of the solver also has a great impact on the accuracy of the final result. In the calculation process, the continuous compression equation and the Reynolds average N-S equation are mainly applied. The static domain includes the flowing airflow and

the support rod of the wind turbine. It needs to simulate the direction and speed of the airflow inflow. The inlet is set to the speed inlet, the moderate turbulence, the wind speed is 1–10 m/s, and the outlet is the pressure outlet. The value is 0. The top and bottom of the static domain are set to walls, and the left and right sides are set to be symmetrical. The rotating domain includes the blades, the connecting shaft and the internal airflow of the wind turbine. It needs to simulate the speed and direction of the rotation of the rotor and select the angular velocity of the rotation of the rotating field according to different TSR (0.1–1). By selecting the semi-implicit method (SIMPLE) of the pressure-dependent equation, the accuracy of the calculation requirements and the fast convergence of the calculation are achieved. This method considers the combination of the high-order solution and the upwind mode, so it is very suitable. The specific simulation parameters are shown in Table 2. In addition, the choice of step size is very critical. If the step size is too short, the calculation result will not converge; the step size is too long, the calculation time is prolonged, and a lot of time is wasted. After a lot of calculation and verification, the model used in this paper achieves the calculation accuracy when the step size reaches 300 steps.

**Table 2.** The solver parameters.

Reynolds Number	Turbulence Model	Iterations	No. of Meshes	Residual Target
$6.0 \times 10^5$	Standard k-e model	300 steps	800,000	$1.0 \times 10^{-4}$

### 2.3. Performance Analysis

In the calculation process, the wind speed of the inflow airflow is held constant at 5 m/s, and the tip speed ratio is changed between 0–1 by changing the corresponding parameters. Figure 7 is a tip speed ratio–wind energy utilization coefficient curve. As shown in Figure 7, the TSR is between 0.1 and 0.7, and with the increase of the TSR, the wind energy utilization rate shows a trend of increasing first and then decreasing. The wind energy utilization coefficient is maximum when the TSR = 0.4. If the rotational speed of the wind turbine is stabilized at this time, the maximum utilization efficiency of wind energy can be achieved.

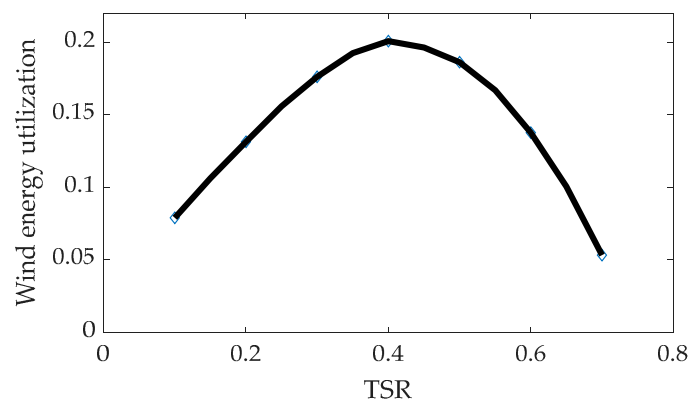


**Figure 7.** Tip speed ratio—wind energy utilization curve.

As shown in Figure 8, by setting TSR = 0.23,  $v_u = 9$  m/s, the torque coefficient comparison curve of the three blades of the wind turbine in one rotation period can be calculated. The scatter point in Figure 8 is the actual data of the simulation calculation, and the fitting curve drawn according to the scatter diagram is roughly three sinusoidal curves, from which it can be concluded that the three blades always have one blade to do the most work. The total output torque of the three blades of the wind turbine is basically stabilized and fluctuates between 4.5–5 N m.

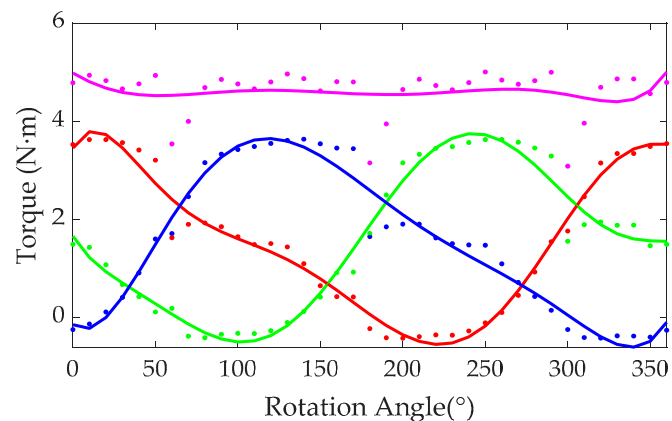


Figure 8. Torque comparison of three blades.

### 3. Structural Optimization

In order to improve the torque coefficient of the wind turbine and find the best structural performance parameters, this paper uses numerical simulation to improve its structure. This section changes the number of blades and the ratio of the major axis to the minor axis radius of the blade inlet portion, and determines whether the wind turbine performance is optimized through simulation calculation. Figure 9a is a three-dimensional model in which the ratio of the major axis of the ellipse to the minor axis radius of the inlet portion of the blade ( $b/a$ ) is constant, and the number of blades is 2, 3, 4 and 5, respectively. Figure 9b is a three-dimensional model in which the number of blades is the same, and the ratio of the major axis to the minor axis radius of the blade inlet portion is 0.38, 0.57 and 0.76, respectively.

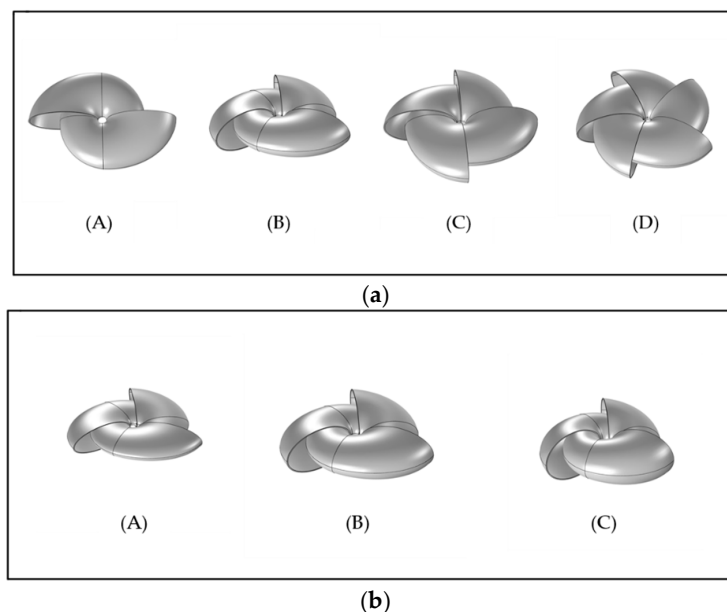


Figure 9. (a) Wind turbine with different number of blades; (b) Wind turbine with different ratio of major axis to minor axis of blade inlet section.

Figure 10 is a pressure distribution contour of the blade when the number of blades is different. The left side is the position rotated by  $0^\circ$ , and the right side is the position rotated by  $60^\circ$ . Figure 10a is a contour showing the pressure distribution of the blade when the number of blades is 2. It can be seen that in the initial position, the outside of the air inlet is facing the wind, and the inlet and the outlet pressure are maximum at this time. When the wind turbine blades rotate, the air inlet gradually receives the incoming air, and the pressure becomes larger. After the wind turbine absorbs

the incoming wind, the blades are facing away from the wind, and the pressure is much smaller than the front of the blades. Figure 10b is a contour showing the pressure distribution of the blade when the number of blades is three. It can be seen that after being driven by the wind energy to rotate for a certain angle, the air inlet will become an air outlet and release unused wind energy. In the initial position and the position after the rotation of 60°, there is always an air inlet facing the wind. However, the two-blade wind turbine has a time period in which the air inlet is facing away from the wind, so the wind energy utilization rate of the three-blade wind turbine is superior to that of the two-blade wind turbine. Figure 10c is a contour showing the pressure distribution of the blade when the number of blades is four. During the rotation of the four-blade wind turbine, only one air inlet is facing the wind, so the wind energy utilization rate is not much better than the three-blade wind turbine. Compared with the three-blade wind turbine, the internal pressure of the wind wheel becomes smaller due to the larger internal space. Figure 10d is a contour showing the pressure distribution of the blade when the number of blades is five. It can be seen that there are two air inlets facing the wind at the same time, which can absorb more incoming wind, and the pressure of the wind wheel will increase, and the wind turbine support rod needs to withstand greater pressure.

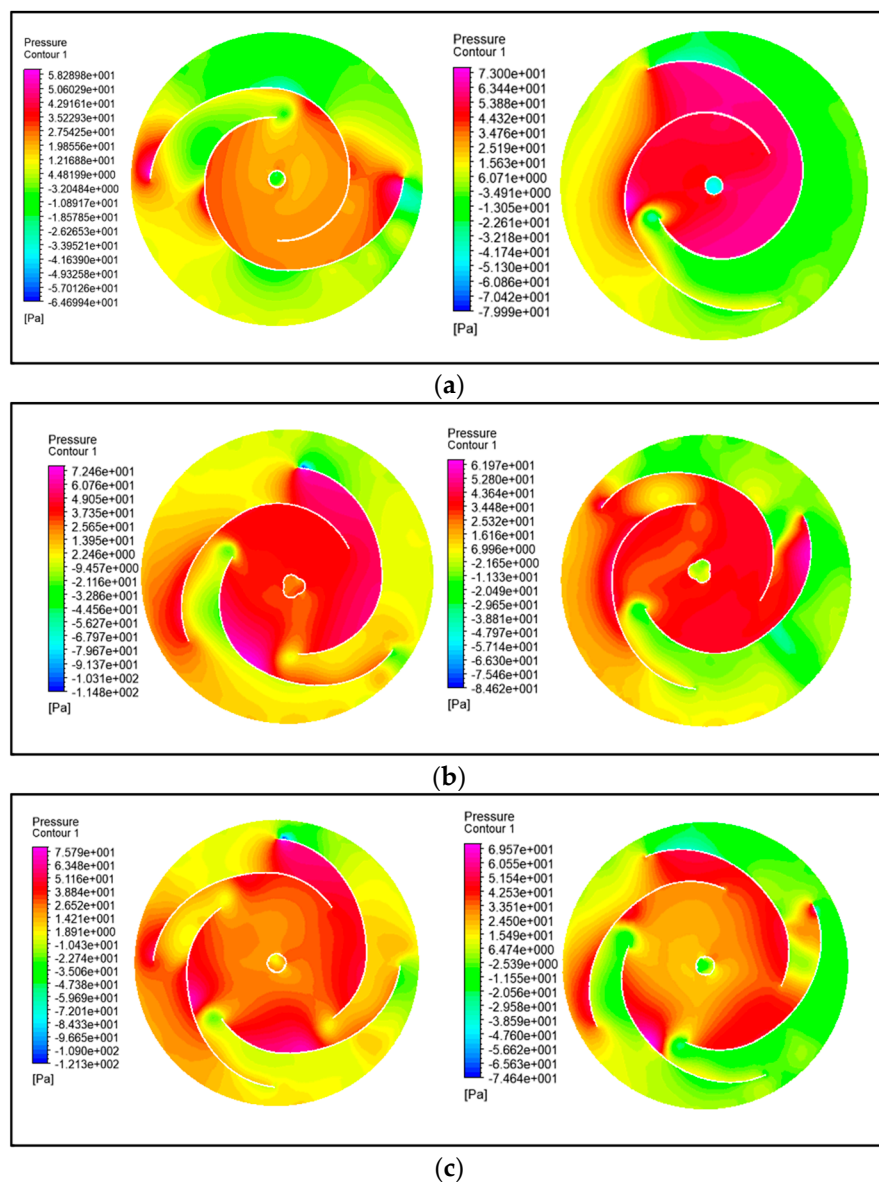
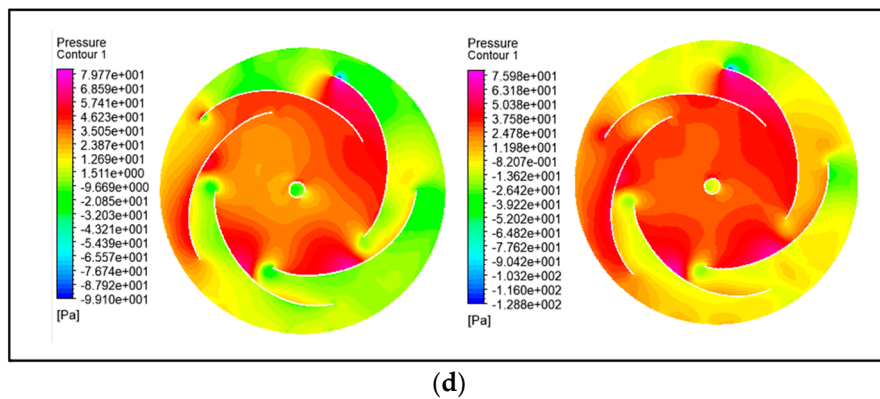
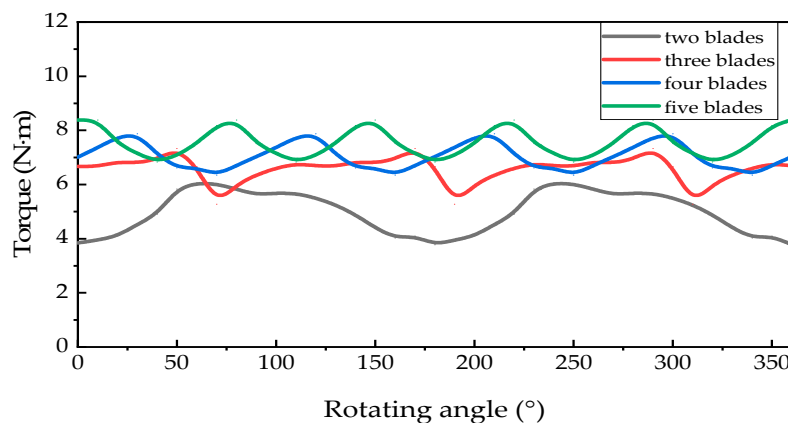


Figure 10. Cont.



**Figure 10.** The pressure distribution contour when the number of wind turbine blades is two, three, four, and five respectively. (a) The number of blades is two; (b) The number of blades is three; (c) The number of blades is four; (d) The number of blades is five.

Figure 11 is a comparison curve of torque generated by one rotation period when the number of blades of the wind turbine is different. As shown in Figure 11, the torque of the two-blade wind turbine is the smallest, and the torque of the other three cases has a small difference in torque. Figure 12 is a comparison curve of wind energy utilization rate when the number of blades is different. From the graph of wind energy utilization coefficient, it can be seen that the maximum wind energy utilization coefficient of three-blade to five-blade is higher, but the duration of the maximum wind energy utilization coefficient of five-blade and four-blade less than three-blade (the range of usable wind speeds is smaller).



**Figure 11.** Torque comparison curve when the number of blades is two, three, four and five.

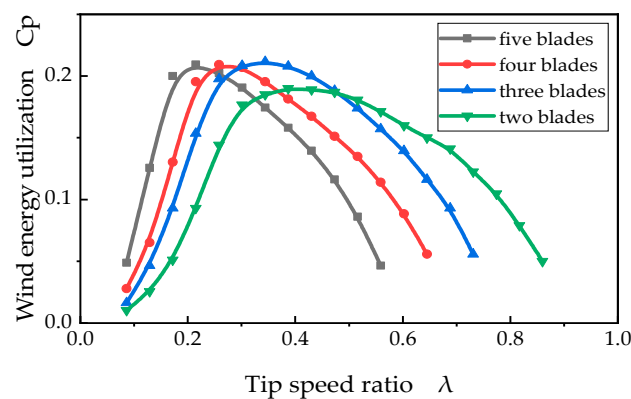


**Figure 12.** Comparison curve of wind energy utilization when the number of blades is two, three, four and five.

The wind turbine hopes that the rotation speed is high, and a high wind energy utilization coefficient can be obtained in a wide range of wind speeds, that is, it can work in a wide range of blade tip speed ratios and operate at a suitable high rotation speed. Figure 13 is a comparison curve of relative flow velocity with the wind turbine as the origin and the incoming flow direction as the X axis. It can be seen from the figure that the two-blade wind turbine absorbs the least amount of wind energy, so that the utilization of wind energy is the smallest; the five-blade wind turbine absorbs the most wind energy, resulting in the highest pressure and has a greater impact on the downstream wake region; the relative velocity of the four-blade wind turbine fluctuates, and the available wind speed range is relatively small, consistent with the above analysis results of pressure profile, torque, and wind energy utilization. The analysis of torque, wind energy utilization and relative velocity is consistent with the analysis of pressure contours, so a three-blade wind turbine can be selected for optimal performance.

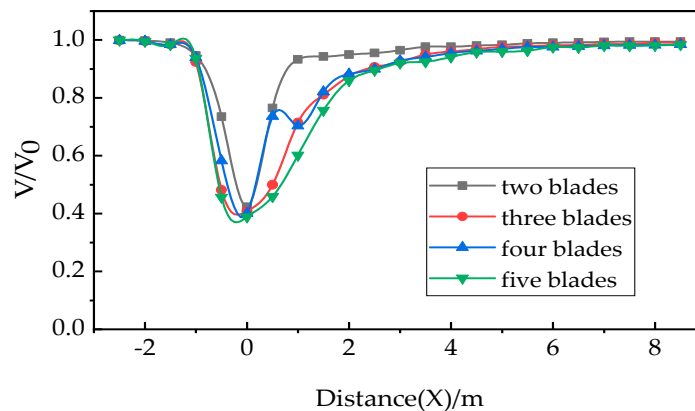


**Figure 13.** Relative velocity comparison curve when the number of blades is two, three, four and five.

The cross section of the air inlet of the blade is an ellipse. After determining the optimal number of blades, the ratio of the size of the air inlet, whether it has an impact on the utilization of wind energy is the next question to be considered. Figure 14 shows the torque obtained by rotating the blade one cycle when the  $b/a$  is different for the three-blade wind turbine. The length of the major axis is constant and the length of the minor axis is increased. The values of  $b/a$  are chosen to be 0.38, 0.57 and 0.76, respectively. As shown in Figure 14, as the ratio of the major axis to the minor axis of the air inlet increases, the torque of the wind turbine increases proportionally, indicating that the value of  $b/a$  has a great impact on the performance of the wind turbine, and it was decided to choose the wind blade at  $b/a = 0.76$ .

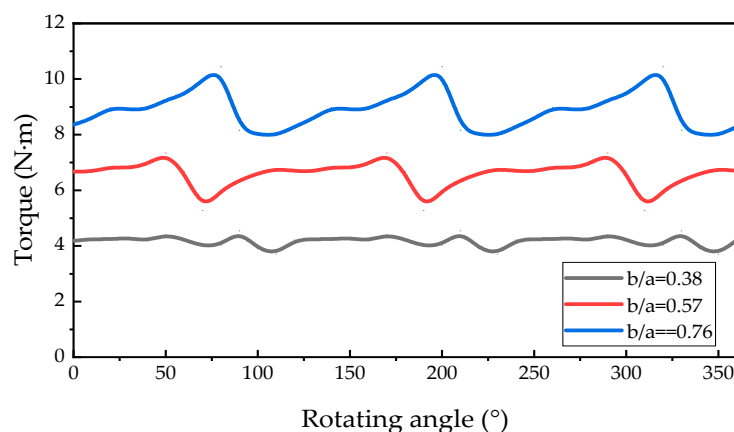


**Figure 14.** Torque comparison curve with different ratios of the major axis to the minor axis.

In order to verify the accuracy of the above analysis, a comparison curve of wind energy utilization ratio and relative flow velocity with different  $b/a$  values were calculated, and the comparison curves are shown in Figures 15 and 16. It can be seen that when  $b/a = 0.38$ , the wind energy utilization rate of the wind turbine is significantly smaller than the other two cases. When  $b/a = 0.57$ , although the wind energy utilization rate at low tip speed ratio is greater than the wind energy utilization rate at  $b/a = 0.76$ , it can be seen that the maximum wind energy utilization rate at  $b/a = 0.76$  is much larger than the other two situations, and its maximum wind energy utilization rate has a wide range of available wind speeds.

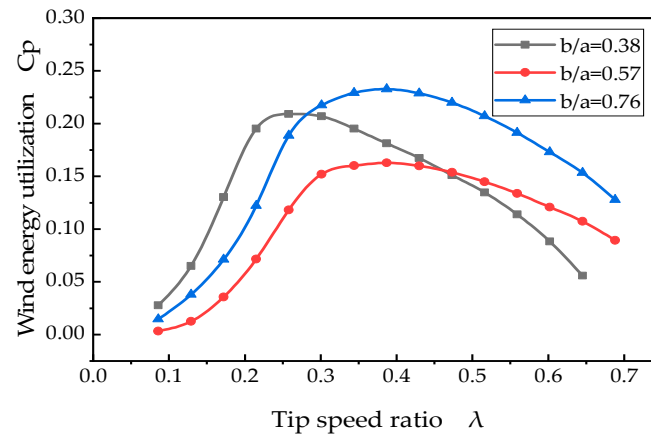


**Figure 15.** Comparison curve of wind energy utilization with different ratios of the major axis to the minor axis.

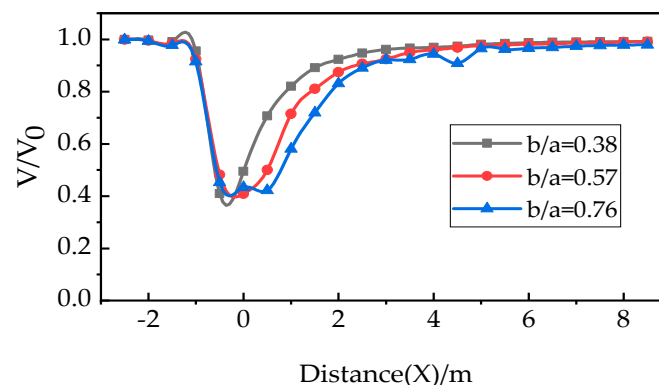


**Figure 16.** Relative velocity comparison curve with different ratios of the major axis to the minor axis.

It can also be seen from the relative velocity comparison curve shown in Figure 15 that  $b/a = 0.76$  absorbs the most wind energy,  $b/a = 0.57$  takes the second place, and  $b/a = 0.38$  absorbs the least wind energy. Based on the above analysis, it is reasonable to select  $b/a = 0.76$ .

#### 4. Wind Turbine Simulation Platform and Experimental Research

##### 4.1. Wind Turbine Simulation Platform

In order to ensure that the Nautilus isometric spiral wind turbine can be applied to the actual power plant, the power generation characteristics of the generator are tested by MATLAB combined with the flow field simulation software. Figure 17 is a system block diagram.

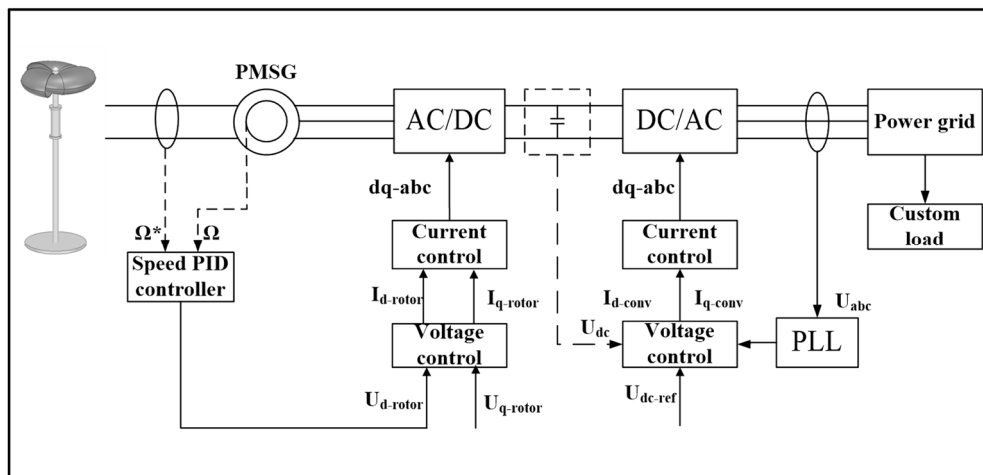


Figure 17. System block diagram.

The dynamic equation of the vertical axis wind turbine shaft to drive the generator rotor is [21–24]:

$$T - T_0 = J \frac{dw}{dt}, \quad (14)$$

where  $T$  is the wind turbine output torque;  $T_0$  is the resistance torque;  $J$  is the moment of inertia;  $w$  is the angular velocity of rotation.

In the generator model, if the center line of the permanent magnet rotor is the  $d$ -axis, the  $q$ -axis is  $90^\circ$  ahead of the rotor rotation direction. The mathematical model of the  $d$ -axis and  $q$ -axis is as follows:

$$u_{sd} = \frac{d\psi_{sd}}{dt} + R_s i_{sd} - \omega_e \psi_{sq}, \quad (15)$$

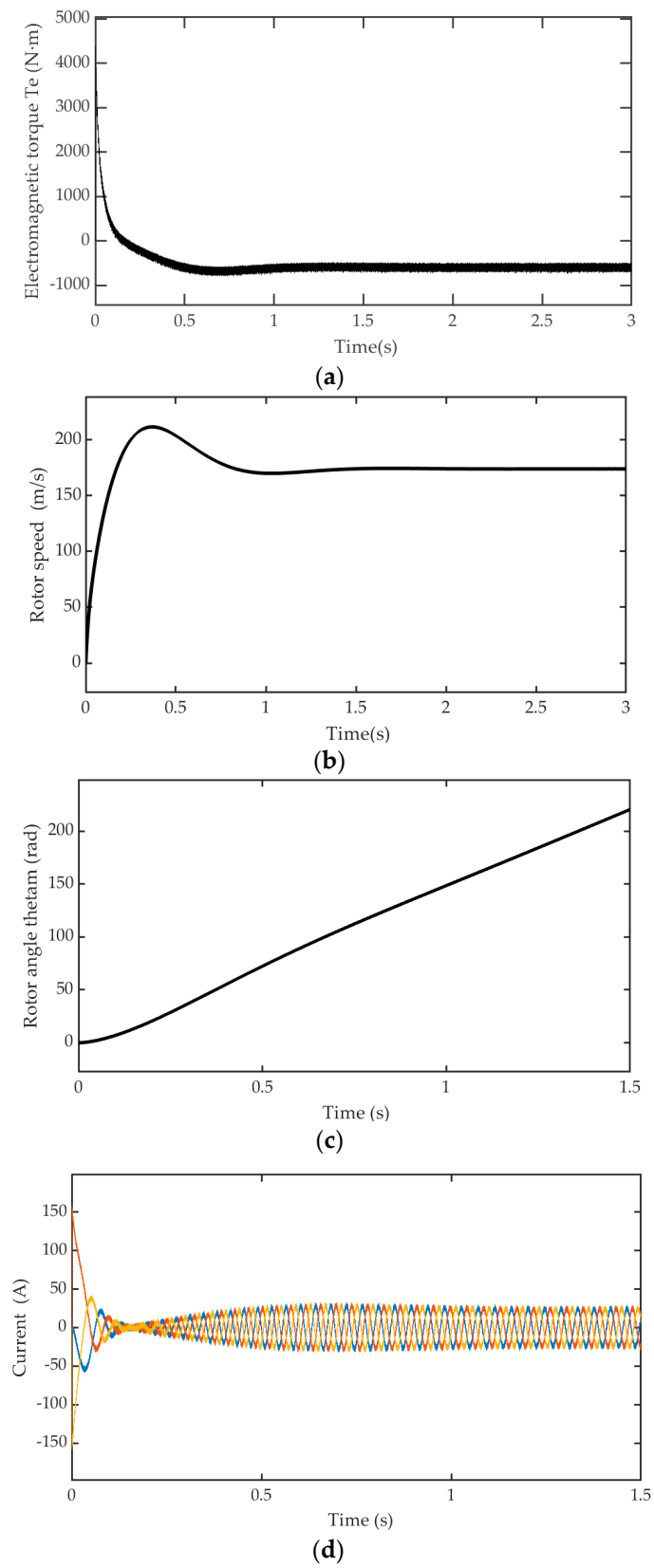
$$u_{sq} = \frac{d\psi_{sq}}{dt} + R_s i_{sq} - \omega_e \psi_{sd}, \quad (16)$$

$$uT_e = 1.5p(\phi_{sd}i_{sq} - \phi_{sq}i_{sd}), \quad (17)$$

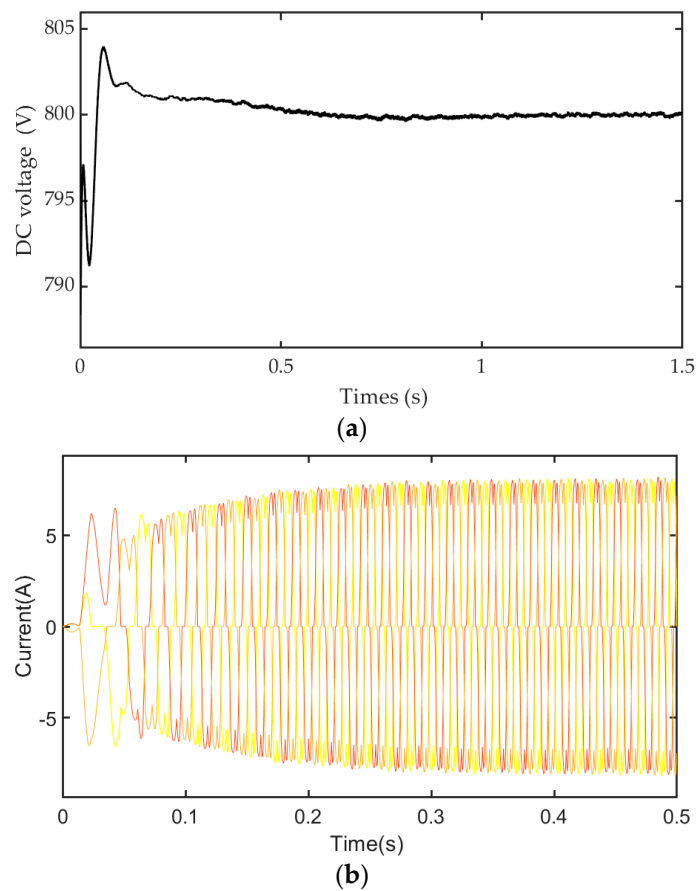
where  $R_s$  is the stator winding phase resistance;  $u_{sd}$ ,  $u_{sq}$  is the motor terminal voltage  $d$ ,  $q$  axis component;  $\psi_{sd}$ ,  $\psi_{sq}$  is the  $d$ ,  $q$  axis component of the stator flux linkage;  $i_{sd}$ ,  $i_{sq}$  is the stator current  $d$ ,  $q$  axis component;  $\omega_e$  is the electrical angular velocity;  $p$  is the number of generator rotor pole pairs.

Figure 18 is a simulation system of the wind power generation and grid-connection process built according to the block diagram of Figure 17. In the simulation module, parameters such as wind speed and wind turbine radius are input, and the generator power generation characteristic curve shown in Figure 19 is obtained. The simulation time is set to 2 s, and Figure 19a is the torque curve of the generator, Figure 19b is the generator speed curve, Figure 19c is the generator rotor angle curve, and Figure 19d is the generator current curve. If you want to convert wind energy into electricity in the national grid for users to use, firstly, it needs to convert the alternating current into direct current through the rotor-side inverter and send it to the national grid side through the direct current transmission system. The DC power transmission process is a key part of it. To ensure the accuracy of this link, the DC voltage of the transmission process is measured in the simulation model of Figure 20. Since the user's electricity is AC, the DC power obtained by the national grid is converted into AC power for users to use after DC/AC conversion and grid-side inverter control. Figure 20a shows the DC voltage curve measured by the direct link, and Figure 20b shows the AC power for the user after rectification. As shown in Figure 20, after the wind turbine is rectified, the voltage and current oscillations are small, and the electrical energy fed back to the grid will not cause a large impact.





**Figure 19.** System block diagram. (a) The torque curve; (b) The speed curve; (c) The rotor angle curve; (d) The current curve.



**Figure 20.** The parameters incorporated into the grid process. (a) The DC voltage incorporated into the grid process; (b) The AC current for the user.

#### 4.2. Experimental Verification

According to the calculation results above, the prototype of the corresponding structural parameters was fabricated to verify the accuracy of the simulation system, the Nautilus isometric spiral wind turbine was installed in the relatively empty area of Alashan, Inner Mongolia. Figure 21a shows the wind turbine prototype running process at a certain moment, the diameter of the wind turbine is 1.3 m. Figure 21b is a comparison curve between measured power and simulated power. It can be seen from the figure that as the wind speed increases, the output power curve obtained by the simulation system is larger than the power measured by the prototype. The reason for this may be due to the wind turbine itself (power loss) and environmental, wind speed, air quality and other factors. These uncontrollable factors are neglected in the simulation study, so there is a certain deviation is reasonable. Moreover, the simulated flow field is ideal. The prototype flow field is affected by complicated factors such as surrounding buildings, which makes the simulation flow field and the actual environment have certain differences, so it is acceptable to have a difference between the simulation result and the actual result.

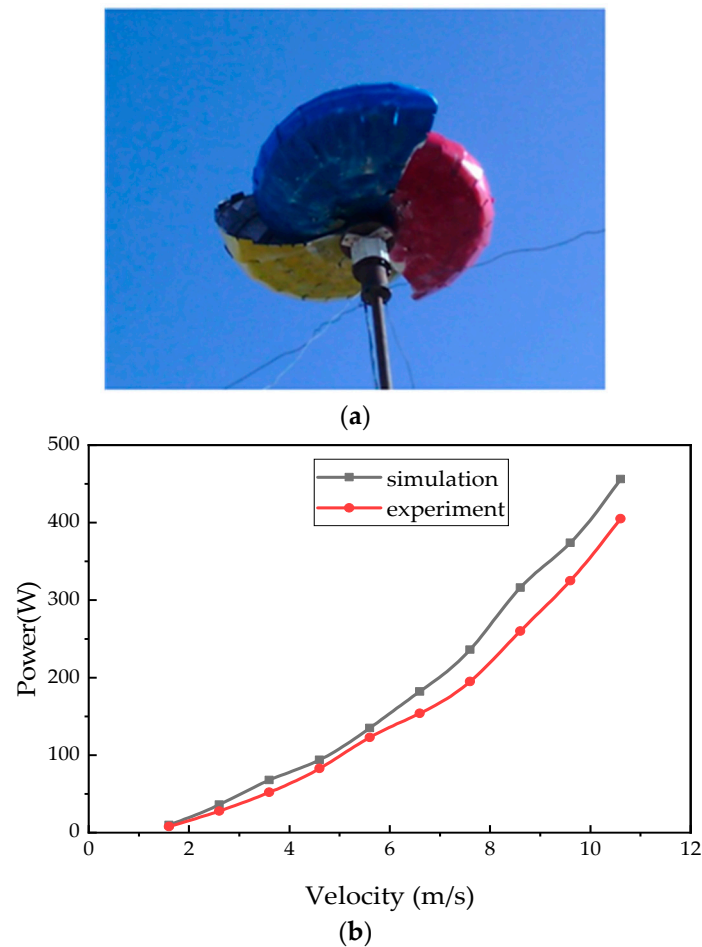


**Figure 21.** (a) Wind turbine prototype; (b) Comparison curve of measured power and simulated power.

## 5. Discussion

The attention to vertical axis wind turbines has gradually increased. How to improve the utilization rate of wind energy and solve the control problems and automatic start problems has become the focus of researchers. In order to improve the utilization of wind energy and solve the problem of automatic startup, some researchers have proposed new vertical axis wind turbine models, and some researchers have analyzed the aerodynamic performance of wind turbines to optimize the original wind turbine Structure [7–9,25–27]. Some researchers have also focused on the difficulty of controlling vertical axis wind turbines. By studying the power generation characteristics of the generator control system and improving the control method, the wind energy conversion efficiency is improved, and the generated electric energy is incorporated into the national power grid [21–24,28–31]. This article draws on the essence of the above two ideas. First, a new Nautilus isometric helical wind turbine structure is proposed. Then, by analyzing the aerodynamic performance, the blade number and blade size are improved. This article draws on the essence of the above two ideas. A new Nautilus isometric spiral wind turbine structure was proposed. By analyzing the aerodynamic performance, the impeller structure parameters (blade number and blade size) were improved, and the wind energy conversion efficiency was improved. Then, by setting up a power generation and grid control platform, the entire basic process from wind energy to grid connection was realized.

Because this wind turbine is a new type of structure and it has high analytical value, this article is only a relatively basic study, and there are many more studies that can be carried out in the future. If this kind of wind turbine is to be applied in practice, it needs to be researched as follows:

First of all, the structural mechanics of the blades and support rods and the stability of the foundation need to be analyzed. Such studies have been widely proposed in the literature [32–37]. Besides, the wake effects of wind turbines need to be analyzed to determine whether they can be applied to wind farms. Such studies have been widely proposed in the literature [2,38].

## 6. Conclusions

In this paper, a three-dimensional model of the Nautilus isometric spiral wind turbine is established, and the simulation software is used for calculation and research. The basic performance parameters such as the wind energy utilization rate and torque of the wind turbine are discussed. On this basis, in order to achieve the optimal design of the Nautilus equidistant spiral wind turbine, two optimization schemes (the number of blades are two, three, four, five and the ratios of the major axis of the ellipse to the minor axis radius of the blade are 0.38, 0.57, 0.76). After comparing parameters such as pressure profile, torque, wind energy utilization and relative speed when the number of blades is different, the optimal number of blades is determined to be three. After comparing parameters such as torque, wind energy utilization, and relative velocity when the blade inlet size is different, the optimal size is determined to be 0.76. The conclusion is that when the number of blades is three and the ratio of the major axis of the ellipse to the minor axis radius of the blade is 0.76, the best performance of this wind turbine can be obtained. In addition, according to the mathematical model of the generator, a simulation platform for power generation and grid-connected control systems was set up. The power generation characteristics of the generator, the grid-connected transmission process, and the stability of the user's electricity were analyzed. Finally, by constructing a wind turbine prototype, the actual power of the wind turbine was measured and compared with the measured power in the simulation, which verified the feasibility and effectiveness of the wind turbine and its subsequent power generation system.

**Author Contributions:** Writing—review and editing, supervision, project administration, funding acquisition, Z.L.; methodology, ANSYS software, writing—original draft preparation, W.Z.; MATLAB software, data curation, H.D.; validation, Y.T. All authors have read and agree to the published version of the manuscript. All authors have read and agreed to the published version of the manuscript.

**Funding:** This research was funded by the National Natural Science Foundation of China, grant No. 51577048, 51877070, the Natural Science Foundation of Hebei Province of China, grant No. E2018208155, the Talent Engineering Training Support Project of Hebei Province of China, grant No. A201905008, the National Engineering Laboratory of Energy-saving Motor & Control Technique, Anhui University, grant No. KFKT201901, Hebei Province Higher Education Science and Technology Research Key Project, grant No. ZD2018228.

**Conflicts of Interest:** The authors declare no conflict of interest.

## References

1. Davidson, M.R.; Zhang, D.; Xiong, W.; Zhang, X.; Karplus, V.J. Modeling the potential for wind energy integration on China's coal-heavy electricity grid. *Nat. Energy* **2016**, *1*, 1–7. [[CrossRef](#)]
2. Tian, J.; Zhou, D.; Su, C.; Soltani, M.; Chen, Z.; Blaabjerg, F. Wind turbine power curve design for optimal power generation in wind farms considering wake effect. *Energies* **2017**, *10*, 395. [[CrossRef](#)]
3. Ma, C.; Song, L.; Zhang, M.Z. Performance study for a novel vertical axis wind turbine based on simulation analysis. In Proceedings of the 14th IEEE International Conference on Networking, Sensing and Control (ICNSC), Calabria, Italy, 16–18 May 2017; pp. 1–6.
4. Magalhaes, A.I.; Matos, F.F.D.S. A characterization of vertical axis wind turbines. *IEEE Lat. Am. Trans.* **2016**, *14*, 4255–4260.
5. Behnam, M.; Aaron, R.; Hu, H.; Anupam, S. Numerical investigation of aerodynamic performance and loads of a novel dual rotor wind turbine. *Energies* **2016**, *9*, 571.
6. Wu, Y.K.; Li, Z.Q.; Zhang, Z.H.; Liu, L. Numerical simulation study on aerodynamic design scheme of megawatt H-type vertical axis wind turbine. *J. Eng. Therm. Energ. Power.* **2019**, *6*, 155–164.
7. Song, L.; Ma, C.; Zhang, M.Z.; Yang, Z.X. Three-dimensional performance of fish-like wing airfoil vertical axis wind turbine. *J. Henan Univ. Sci. Technol.* **2018**, *39*, 12–16.

8. Chen, L.; Mo, Q.Y.; Yin, J.P.; Liu, W.; Jiang, L.; Liao, Z. Aerodynamic performance analysis of integrated wind turbine with deflector. *Mach. Des. Res.* **2019**, *35*, 205–209.
9. Cai, X.; Hu, L.; Ding, W.X.; Zhu, X.P. Study on aerodynamic characteristics of a new lift-drag hybrid vertical axis wind turbine. *China. J. Comput. Mech.* **2019**, *36*, 555–561.
10. Sunny, K.A.; Kumar, P.; Kumar, N.M.; Banerjee, J.; Adheena, G.J. Airfoil selection and computational study on the torque performance of 4-blade vertical axis wind turbine. *J. Phys. Conf. Ser.* **2018**, *1139*, 012040. [[CrossRef](#)]
11. Almohammadi, K.M.; Ingham, D.B.; Ma, L.; Pourkashanian, M. 2-D-CFD analysis of the effect of trailing edge shape on the performance of a straight-blade vertical axis wind turbine. *IEEE Trans. Sustain. Energy* **2015**, *6*, 228–235. [[CrossRef](#)]
12. Tian, W.L.; Song, B.W.; Mao, Z. Numerical calculation of aerodynamic performance of Savonius-type wind turbine with elliptical blades. *Proc. Chin. Soc. Elect. Eng.* **2014**, *34*, 5796–5802.
13. Zhao, Z.G.; Wang, T.G.; Huang, J.; Ye, F.; Zheng, Y.; Zhao, Z. Analysis of influence of aerodynamic performance of installation angle on vertical axis wind wheel. *Proc. CSEE* **2014**, *8*, 1304–1309.
14. Xu, L.; Li, X.M.; Qu, J.J. Effects of blade number and chord length on lift-type vertical axis wind turbine. *Renew. Energy Res.* **2016**, *34*, 1834–1840.
15. Li, Z.; Han, R.; Gao, P.; Wang, C. Analysis and implementation of a drag-type vertical-axis wind turbine for small distributed wind energy systems. *Adv. Mech. Eng.* **2019**, *11*. [[CrossRef](#)]
16. Zhang, M.; Wang, L.; Xu, J. Research on compound control strategy of wind/PV/storage hybrid power generation system. *High Vol. Appar.* **2018**, *54*, 64–72.
17. Yang, B.; Yu, T.; Shu, H.; Zhang, Y.; Chen, J.; Sang, Y.; Jiang, L. Passivity-based sliding-mode control design for optimal power extraction of a PMSG based variable speed wind turbine. *Renew. Energ.* **2018**, *119*, 577–589. [[CrossRef](#)]
18. Das, A.; Chimonyo, K.B.; Kumar, T.R.; Gourishankar, S.; Rani, C. Vertical axis and horizontal axis wind turbine—A comprehensive review. In Proceedings of the International Conference on Energy, Communication, Data Analytics and Soft Computing, Nadu, India, 1–2 August 2017; pp. 2660–2669.
19. Tian, Y. Nautilus Isometric Spiral Wind Turbine Generator. CN 106368896A. 1 February 2017.
20. Meng, Y.W. The Experimental and Numerical Simulation of Wind Turbine Flow Field in a Find Tunnel. Master's Thesis, Tianjin University, Tianjin, China, 2017.
21. Li, Z.; Gao, P.; Sun, T.; Xue, Z.; Wang, Q. Numerical simulation and analysis of characteristics of drag type vertical axis wind turbine for distributed energy system. *Trans. China Electrotech. Soc.* **2017**, *32*, 155–163.
22. Kong, L.; Cai, G.; Chen, C.; Xing, L. Modeling and grid-connected control of proactive permanent magnet direct-driven wind turbine based on energy storage of hydrogen. *Trans. China Electrotech. Soc.* **2017**, *18*, 276–285.
23. Li, Z.; Sun, T.; Gao, P.F. The simulation analysis of vertical axis wind turbine characteristics for distributed generation system. *J. Electr. Eng.* **2016**, *5*, 89–92.
24. Cai, G.W.; Kong, L.G.; Pan, C.; Yang, D.Y.; Sun, Z. Modeling and grid-connected control strategy for wind and light storage combined power generation system. *J. Electr. Eng.* **2013**, *28*, 196–204.
25. Jin, X.; Gan, Y.; Yang, X.G.; Ju, W. Performance optimization of vertical axis wind turbine with baffles. *Acta Energ. Sol. Sin.* **2018**, *28*, 1995–2002.
26. Hu, R.H.; Li, H.X.; Wang, Y.W.; Fan, C.; Ma, Z. Design and manufacturing technology of a new type of small vertical axis wind turbine blade. *Renew. Energ. Res.* **2013**, *31*, 73–76.
27. Richard, J.P.; Larry, B. Toward the coevolution of novel vertical-axis wind turbines. *IEEE Trans. Evol. Comput.* **2015**, *19*, 284–294.
28. Brain, H.; Andrew, C.; Ger, K. A low-order model for offshore floating vertical axis wind turbine aerodynamics. *IEEE Trans. Ind. Appl.* **2017**, *53*, 512–520.
29. Liu, S.L.; Sun, H.S.; Gu, M.L.; Wen, J. Grid-connected operation control of a new wind turbine and flywheel energy storage combined system. *J. Electr. Eng.* **2012**, *27*, 248–254.
30. Ma, Z.; Yan, Z.; Shaltout, M.L.; Chen, D. Optimal real-time control of wind turbine during partial load operation. *IEEE Trans. Cont. Syst. Technol.* **2015**, *23*, 2216–2226. [[CrossRef](#)]
31. Ming, H.Y.; Yan, X.; Chun, S.; Liu, J.K.; Zhao, Y.D. Turbine stability-constrained available wind power of variable speed wind turbines for active power control. *IEEE Trans. Power Syst.* **2017**, *32*, 2487–2488.
32. Elias, S.; Matsagar, V.; Datta, T.K. Distributed multiple tuned mass dampers for wind response control of chimney with flexible foundation. *Procedia Eng.* **2017**, *199*, 1641–1646. [[CrossRef](#)]

33. Tazi, N.; Chatelet, E.; Bouzidi, Y. Using a hybrid cost-FMEA analysis for wind turbine reliability analysis. *Energies* **2017**, *10*, 276. [[CrossRef](#)]
34. Bayat, M.; Andersen, L.V.; Ibsen, L.B. *p-y-y* curves for dynamic analysis of offshore wind turbine mono-pole foundations. *Soil Dyn. Earthq. Eng.* **2016**, *90*, 38–51. [[CrossRef](#)]
35. Andersen, L.V. Dynamic soil–structure interaction of poly-pod foundations. *Comput. Struct.* **2018**, *7*, 105966. [[CrossRef](#)]
36. Elias, S. Engineering effect of SSI on vibration control of structures with tuned vibration. *Shock Vib.* **2019**, *2019*, 7463031. [[CrossRef](#)]
37. Elias, S.; Matsagar, V.; Datta, T.K. Along-wind response control of chimneys with distributed multiple tuned mass dampers. *Struct. Control Health Monit.* **2019**, *26*, e2275. [[CrossRef](#)]
38. Okulov, V.L.; Naumov, I.V.; Mikkelsen, R.F.; Sørensen, J.N. Wake effect on a uniform flow behind wind-turbine model. *J. Phys. Conf. Ser.* **2015**, *625*, 1–8. [[CrossRef](#)]



© 2019 by the authors. Licensee MDPI, Basel, Switzerland. This article is an open access article distributed under the terms and conditions of the Creative Commons Attribution (CC BY) license (<http://creativecommons.org/licenses/by/4.0/>).